

## Cross-scale operational oceanography in the Adriatic Sea

Christian Ferrarin<sup>a</sup>, Silvio Davolio<sup>b</sup>, Debora Bellafiore<sup>a</sup>, Michol Ghezzi<sup>a</sup>, Francesco Maicu<sup>a</sup>, William Mc Kiver<sup>a</sup>, Oxana Drofa<sup>b</sup>, Georg Umgiesser<sup>a</sup>, Marco Bajo<sup>a</sup>, Francesca De Pascalis<sup>a</sup>, Piero Malguzzi<sup>b</sup>, Luca Zaggia<sup>a</sup>, Giuliano Lorenzetti<sup>a</sup>, and Giorgia Manfè<sup>a</sup>

<sup>a</sup>CNR - National Research Council of Italy, ISMAR - Marine Sciences Institute in Venice, Castello 2737/f, 30122, Venice, Italy; <sup>b</sup>CNR - National Research Council of Italy, ISAC - Institute of Atmospheric Sciences and Climate in Bologna, Via Gobetti 101, 40129, Bologna, Italy

### ARTICLE HISTORY

Compiled January 24, 2019

### ABSTRACT

The oceanographic forecast capability in coastal seas is often limited by the capacity of the numerical models in correctly reproducing the complex morphology of the coastline and the exchange processes between the shelf and the open seas. In the marginal Adriatic Sea this task is of uppermost importance due to the presence of several coastal water bodies and rivers. We present here a new operational oceanographic system, called Tiresias, based on the unstructured grid model SHYFEM and representing the whole Adriatic Sea together with the lagoons of Marano-Grado, Venice and Po Delta. The novelty of this oceanographic system resides in the very high-resolution, up to 10 m, of the numerical mesh, and in the high spatial and temporal resolution of the forcing and boundary conditions that drive the forecasts. The forecast results are evaluated against sea temperature and salinity profiles, mean circulation fields derived from a regional ocean model, tide gauges and drifter trajectory. The presented results highlighted the capacity of Tiresias in forecasting the general circulation in the Adriatic Sea, as well as several relevant coastal dynamics, such as saltwater intrusion, storm surge and riverine waters dispersion.

### KEYWORDS

Adriatic Sea; Lagoons; Finite element model; Coastal dynamics

## 1. Introduction

2 Oceanographic models are applied worldwide within predictive systems to forecast  
3 the sea state with the aim of helping people to operate more effectively and safely  
4 along the coast and in the open sea. Coastal ocean forecasts are crucial for managing  
5 storm damages and flooding, fisheries and aquaculture activities, shipping, harmful  
6 algal blooms and oil spills (Chaumillon et al. 2017).

7 Simulation of water circulation and of the principal physical processes affecting  
8 coastal areas requires the use of both numerical models at high spatial and tem-  
9 poral resolution and downscaling techniques capable of reproducing mass exchange  
10 between the coastal area and the open sea (coastal-offshore interactions). This goal

11 can be achieved through the implementation of numerical models based on a unique  
12 unstructured grid able to describe processes at different spatial scales (Cucco et al.  
13 2012; Zhang et al. 2016; Ferrarin et al. 2016; Stanev et al. 2017; Federico et al. 2017;  
14 Ferrarin et al. 2018), or through nesting of models (structured and unstructured) at  
15 different resolution (Kourafalou et al. 2015; Trotta et al. 2016, 2017; Fortunato et al.  
16 2017). The use of an unstructured grid gives the advantage of using higher resolution  
17 at the coasts while applying more modest resolution in the deep sea, an approach that  
18 has proved to be accurate for the Adriatic Sea (McKiver et al. 2016).

19 In addition to the appropriate model resolution and numerics, oceanographic oper-  
20 ational systems require the integration with near real-time observations to achieve a  
21 comprehensive description of the dynamics in the coastal sea (Kourafalou et al. 2015;  
22 Wilkin et al. 2017). In operational oceanography, in-situ and remote observations are  
23 needed for the accurate initial estimates of the ocean state to be used for the ini-  
24 tialisation of short-range forecasts (Martin et al. 2015) and to set-up the appropriate  
25 boundary conditions for the simulations. This last requirement is of particular rele-  
26 vance in coastal seas affected by rivers and related buoyancy-driven flows (Kourafalou  
27 et al. 2015). In these systems, the representations of the river plume dynamics is crucial  
28 to achieve reliable coastal ocean forecasts.

29 In the context of operational oceanography, the Adriatic Sea represents a challenge,  
30 given that it is a regional sea strongly affected by air-sea, land-sea, and coastal-offshore  
31 interactions. Indeed, the main forcings of the basin circulation are the wind (influenced  
32 by the complex local orography and small scale processes), the strong buoyancy result-  
33 ing from the freshwater inputs injected by the rivers, and the tidal waves generated in  
34 the Mediterranean Sea (Orlić et al. 1992).

35 The Adriatic Sea is an 800 km long, 150 km wide elongated semi-enclosed basin  
36 communicating with the Mediterranean Sea through the Otranto Strait in the southern  
37 part (Fig. 1). The Adriatic Sea can be formally subdivided, based on its bathymetry,  
38 in the relative shallow northern Adriatic (north of the 100 m-isobath), a middle trench  
39 and the deep southern Adriatic Pit (with depths exceeding 1,000 m, Artegiani et al.  
40 1997). Several shallow coastal transitional water bodies are present in the northern  
41 part of the Adriatic Sea, the main of which are the Marano-Grado Lagoon, the Venice  
42 Lagoon and the system of lagoons of the Po Delta. Such coastal environments have an  
43 average depth of 1.2 -1.5 m and are characterised by a complicated network of channels  
44 (up to 15 m deep), shallow flats (generally about 1 m deep) and marshes, that are  
45 intermittently dry and wet. It has been recently demonstrated by Ferrarin et al. (2017)  
46 that these coastal lagoons significantly influence the tidal induced circulation in the  
47 entire northern Adriatic Sea.

48 Several oceanographic operational systems have been implemented in the Mediter-  
49 ranean and the Adriatic seas during the last two decades (Napolitano et al. 2016;  
50 Coppini et al. 2017, and references therein). The SHYFEM model in barotropic ver-  
51 sion has been implemented at the Centro Previsioni e Segnalazioni Maree (<https://www.comune.venezia.it/it/content/la-previsione>, Bajo and Umgiesser 2010;  
52 Zampato et al. 2016), at the Italian Institute for Environmental Protection and  
53 Research ([http://www.isprambiente.gov.it/pre\\_meteo\\_eng/simm\\_eng.html](http://www.isprambiente.gov.it/pre_meteo_eng/simm_eng.html)) and  
54 at the CNR-ISMAR (<http://www.ismar.cnr.it/kassandra>, Ferrarin et al. 2013)  
55 for forecasting the sea level. However, these systems do not consider the baroclinic  
56 circulation, as they are mainly focused on storm surge and wave forecasting. Full  
57 baroclinic oceanographic forecasts for the Adriatic Sea are available through the  
58 Mediterranean Forecasting System (<http://medforecast.bo.ingv.it/>, Oddo et al.  
59 2009), the Adriatic Forecasting System (<http://www.oceanlab.cmcc.it/afs/>, Oddo  
60 2009).

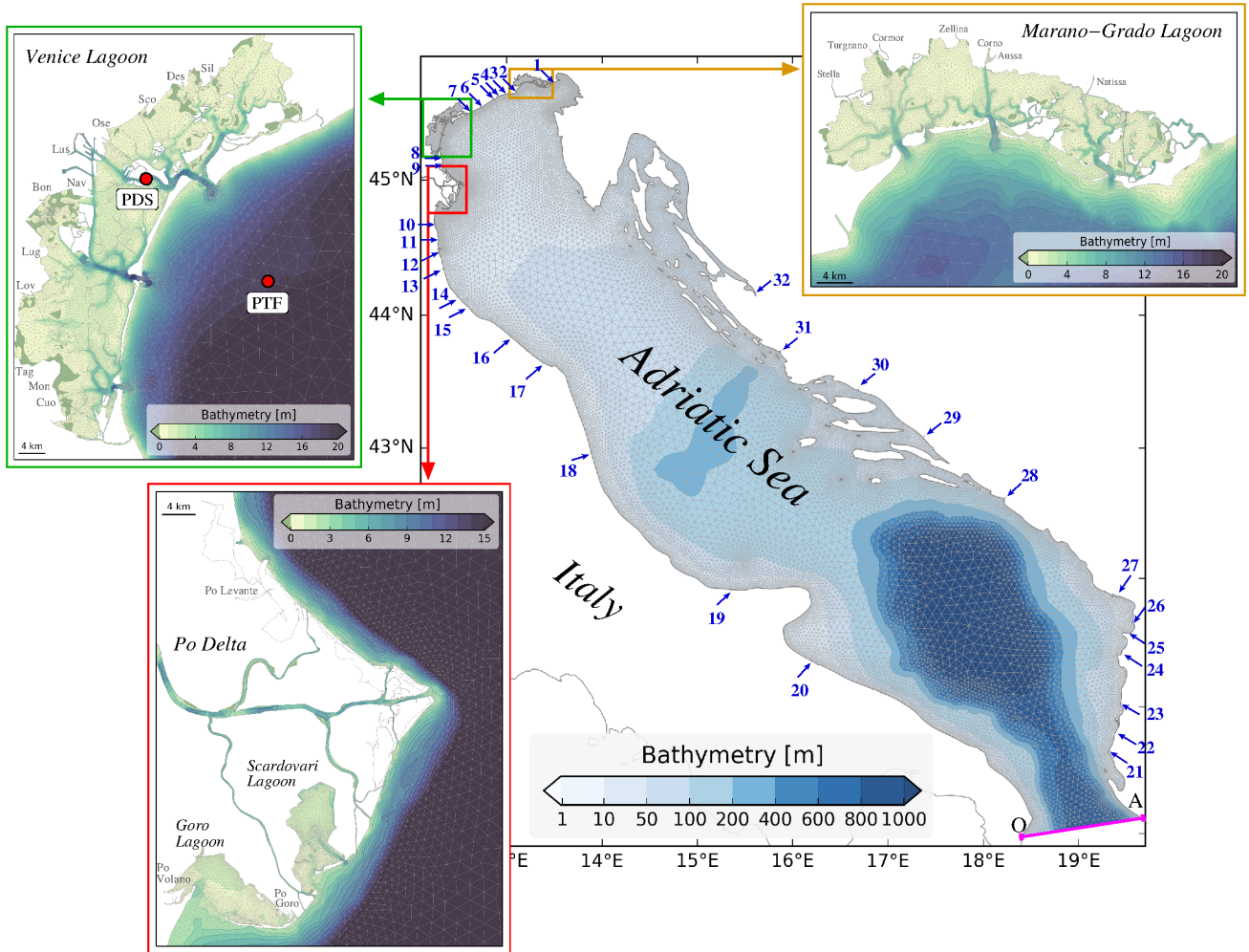


**Figure 1.** Bathymetry of the Adriatic Sea and of the Marano-Grado, Venice and Po Delta lagoons interpolated on the triangular numerical grid (superimposed). Arrows mark the location of the major rivers of the Adriatic Sea: 1) Isonzo, 2) Tagliamento, 3) Canale dei Lovi, 4) Lemene, 5) Livenza, 6) Piave, 7) Sile, 8) Brenta, 9) Adige, 10) Reno, 11) Lamone, 12) Fiumi Uniti, 13) Savio, 14) Uso, 15) Marecchia, 16) Metauro, 17) Esino, 18) Tronto, 19) Fortore, 20) Ofranto, 21) Vijuse, 22) Seman, 23) Shkumbi, 24) Erzen, 25) Ishm, 26) Mat, 27) Bojana, 28) Ombla, 29) Neretva, 30) Cetina, 31) Krka, 32) Zrmanja. Rivers flowing in the lagoons and in the Po Delta are labelled in the zoom panels. The purple OA line indicates the Otranto Strait boundary. The red dots in the upper-left panel indicate the tide gauges used for the storm surge validation.

61 et al. 2006), the BORA Adriatic Marine Forecast (<http://www.bora.gekom.hr>), the  
 62 AdriaROMS Ocean Model Forecast (<https://www.arpae.it/sim/>, Chiggiato and  
 63 Oddo 2008), and the southern Adriatic northern Ionian coastal Forecasting System  
 64 (<http://oceanlab.cmcc.it/sanifs/>, Federico et al. 2017).

65 In this study we describe a novel forecasting system - called Tiresias - for the Adriatic  
 66 Sea and its northern lagoons. With respect to the above cited forecasting systems,  
 67 Tiresias realises a seamless transition between different spatial scales, from lagoon's  
 68 tidal channels to open-sea, and adopts high spatial and temporal resolution of the  
 69 forcing and boundary conditions that drive the forecasts. Tiresias is evaluated against  
 70 observations in both the open sea and the coastal areas, illustrating the capability  
 71 of this tool in forecasting the general circulation features in the Adriatic, as well as  
 72 coastal storm surge, saltwater intrusion and particle dispersion.

## 73 2. The Tiresias forecasting system for the Adriatic Sea

### 74 2.1. The hydrodynamic model

75 The 3D hydrodynamic finite element model SHYFEM solves the primitive equations,  
76 vertically integrated over each layer considering tidal, atmospheric and density-driven  
77 forces. SHYFEM is open source and freely available on the web pages <http://www.ismar.cnr.it/shyfer> and <https://github.com/SHYFEM-model>. SHYFEM has been  
78 already applied to simulate hydrodynamics in the Mediterranean Sea (Cucco et al.  
79 2012; Ferrarin et al. 2013), in the Adriatic Sea (Bellafiore and Umgiesser 2010; Federico  
80 et al. 2017; Ferrarin et al. 2016, 2017), in several coastal systems (Umgiesser et al. 2014,  
81 and references therein) and recently in the Po River-Delta-Sea system (Maicu et al.  
82 2018).  
83

84 The horizontal discretization of the state variables is carried out with the finite  
85 element method, with the subdivision of the numerical domain in triangles varying  
86 in form and size. Velocities are computed in the centre of the grid element, whereas  
87 the water levels are computed at the element vertices (nodes). Vertically the model  
88 applies  $Z$  layers with varying thickness. Most variables are computed in the center  
89 of each vertical layer, whereas stress terms and vertical velocities are solved at the  
90 interfaces between layers.

91 McKiver et al. (2016) pointed out the irrelevance of non-hydrostatic processes for  
92 the northern Adriatic Sea. However, non-hydrostatic processes can play a role in accu-  
93 rately capturing dense water cascading events in the deep Pit in the Southern Adriatic  
94 (Bellafiore et al. 2018), though including such processes comes with a high numerical  
95 cost (approx 4 times the running time of the hydrostatic case), making it impractical  
96 for operational forecasts.

97 The model uses a semi-implicit algorithm for integration over time, which has the ad-  
98 vantage of being unconditionally stable with respect to gravity waves, bottom friction  
99 and Coriolis terms, and allows transport variables to be solved explicitly. The Coriolis  
100 term and pressure gradient in the momentum equation, and the divergence terms in  
101 the continuity equation are treated semi-implicitly. Bottom friction and vertical eddy  
102 viscosity are treated fully implicitly for stability reasons, while the remaining terms  
103 (advective and horizontal diffusion terms in the momentum equation) are treated ex-  
104 plicitly. A more detailed description of the model equations and of the discretization  
105 method is given in Umgiesser et al. (2004) and Ferrarin et al. (2017).

### 106 2.2. The model set-up

107 The numerical computation is performed on a spatial domain that represents the whole  
108 Adriatic Sea, the lagoon of Marano-Grado, the lagoon of Venice and the Po River Delta  
109 (including the Scardovari and Goro lagoons) by means of the unstructured grid shown  
110 in Fig. 1. The numerical domain comprises all Po River branches starting downstream  
111 the Po di Goro diversion (40 km upstream) with 9 river mouths. To adequately resolve  
112 the river-sea continuum, the unstructured grid also includes the lower part of the other  
113 major rivers flowing into the Adriatic Sea.

114 The use of elements of variable sizes, typical of finite element methods, is fully ex-  
115 ploited, in order to suit the complicated geometry of the basin, the rapidly varying  
116 topographic features, and the complex bathymetry of the lagoon systems. The nu-  
117 merical grid of the Adriatic Sea with the lagoons consists in approximately 110,000  
118 triangular elements with a resolution that varies from 7 km in the open-sea to few hun-

119 dred meters along the coast and tens of meters in the inner lagoon channels. Recently,  
120 Ferrarin et al. (2017) showed that the inclusion of the lagoons in the simulation im-  
121 proved the capability of the model in reproducing tidal currents in the whole northern  
122 Adriatic Sea.

123 The model is able to work with wetting and drying, a feature needed in the shallow  
124 lagoons, where some areas consists of salt marshes that are intermittently dry and  
125 wet, and in the Po River floodplains.

126 Because of the wide area, the bathymetry of the Adriatic and the lagoons was  
127 obtained by merging several datasets, having different spatial resolution and obtained  
128 using different measurement approaches, but the same reference datum (Genoa 1942 -  
129 IGM42). The resulting bathymetry, interpolated and superimposed on the triangular  
130 mesh, is shown in Fig. 1.

131 In this model application, the water column is discretised in 34 vertical layers with  
132 variable thickness ranging from 1 m, in the topmost 10 m, to 100 m for the deepest  
133 layer of the Adriatic Sea. The vertical discretization of the surface layers allows one to  
134 describe the tidal propagation over the shallow tidal flats and the vertical structure of  
135 the tidal flow in the tidal channel network. The bottom drag coefficient is computed  
136 using a logarithmic formulation via bottom roughness length, set homogeneous over  
137 the whole system to a value of 0.01 m (Ferrarin et al. 2017).

138 For the free surface, a water flux is used containing evaporation minus precipitation  
139 and river discharge. For computing the water temperature, the air-sea heat fluxes are  
140 parameterised by the COARE (Coupled Ocean-Atmosphere Response Experiment)  
141 3.0 bulk algorithm (Fairall et al. 2003). Also the drag coefficient for the momentum  
142 transfer of wind in the hydrodynamic model is computed according to the COARE  
143 3.0 bulk formulae (Fairall et al. 2003).

### 144 *2.3. Operational forcing and boundary conditions*

145 Reliable forcing and boundary conditions are crucial to correctly forecast the circula-  
146 tion in the Adriatic Sea, which is strongly influenced by high temporal and spatial  
147 variability of the atmospheric conditions and river runoff (Orlić et al. 1992; Artegiani  
148 et al. 1997; Davolio et al. 2015; Brando et al. 2015).

#### 149 *2.3.1. Meteorological forcing*

150 The weather in the Adriatic area is strongly influenced by local orography and small  
151 scale processes, and therefore for realistic oceanographic prediction an appropriate  
152 spatial resolution of the meteorological fields is required (Pasarić et al. 2009). The  
153 use of high-resolution meteorological models is essential to capture the temporal and  
154 spatial inhomogeneity of northeasterly Bora winds, characterised by topographically  
155 controlled high-speed wind jets along the eastern shore (Dorman et al. 2006; Davolio  
156 et al. 2015).

157 In Tiresias, the meteorological forcing is supplied by the MOLOCH limited-area,  
158 high-resolution model, developed and implemented at CNR-ISAC (National Research  
159 Council of Italy - Institute of Atmospheric Sciences and Climate) with a daily opera-  
160 tional chain (<http://www.isac.cnr.it/dinamica/projects/forecasts>). The fore-  
161 cast framework comprises the hydrostatic model BOLAM (implemented over the  
162 Euro-Mediterranean region) and the non-hydrostatic model MOLOCH (implemented  
163 over Italy), nested in BOLAM (Fig. 2). The initial and boundary conditions for the  
164 BOLAM model are derived from the analyses (00 UTC) and forecasts of the GFS

165 (NOAA/NCEP, USA) global model (<http://www.emc.ncep.noaa.gov/GFS>).

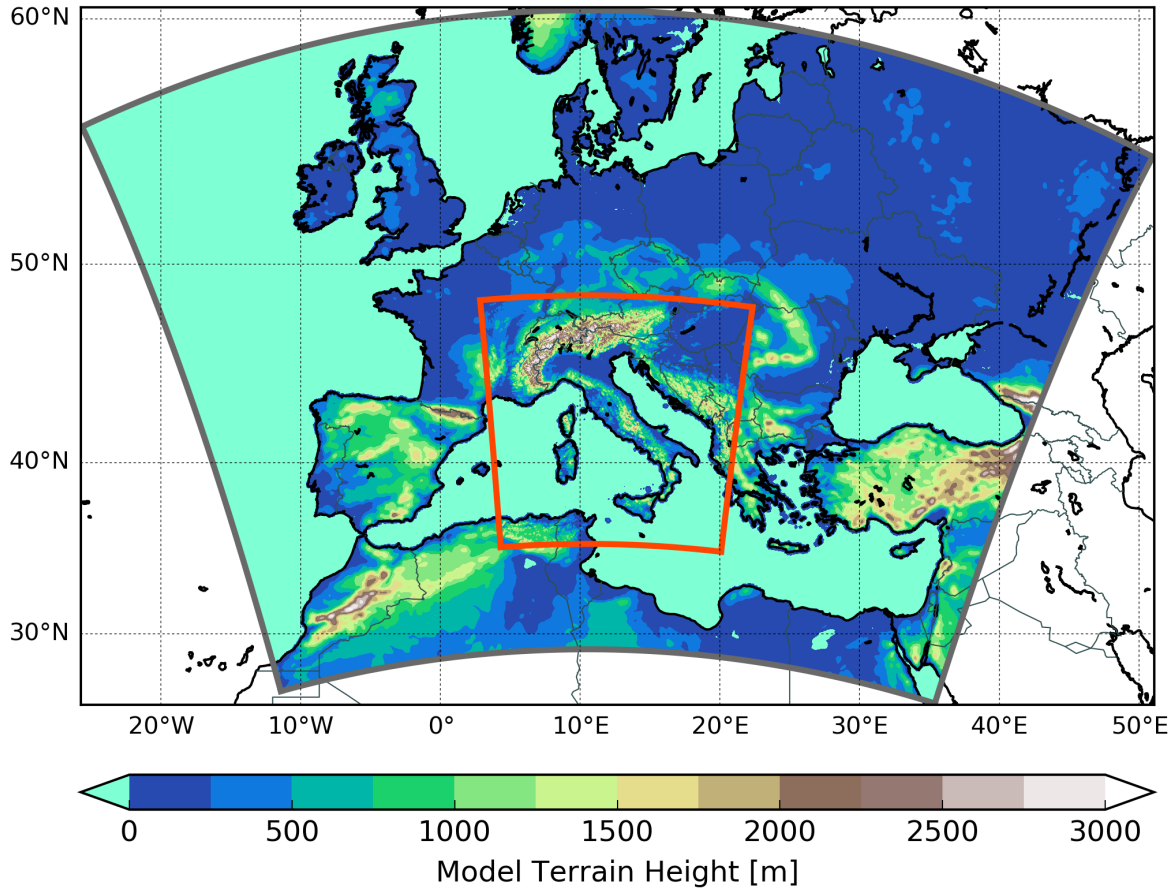


**Figure 2.** Integration domains of the BOLAM (gray box) and MOLOCH (red box) meteorological models.

166 MOLOCH is a non-hydrostatic, fully compressible, convection-permitting model.  
167 The prognostic variables, namely pressure, air temperature, specific humidity, hori-  
168 zontal and vertical wind velocity components, turbulent kinetic energy and five water  
169 species, are represented on a latitude-longitude rotated Arakawa C-grid. It employs  
170 a hybrid terrain-following coordinate, which relaxes to horizontal surfaces at higher  
171 elevation from the ground. Time integration is based on a time-split scheme with an  
172 implicit treatment of the vertical propagation of sound waves and a forward-backward  
173 scheme for the horizontal propagation of gravity and sound waves. Advection is com-  
174 puted using a second order implementation of the Godunov (1959) method, which is  
175 particularly suited to integrate in time the conservation of a scalar quantity (Toro  
176 1992). This scheme is a total variation diminishing one, and therefore prevents the  
177 occurrence of spurious oscillations. See Malguzzi et al. (2006), Buzzi et al. (2014)  
178 and Davolio et al. (2017) for further details about the MOLOCH model physics and  
179 numerics.

180 The MOLOCH model is implemented with a horizontal grid spacing of 0.0113 de-  
181 grees, equivalent to 1.25 km, and with 60 atmospheric levels and 7 soil levels. This  
182 model chain has already been successfully validated over the Adriatic Sea (Davolio  
183 et al. 2015, 2017; Stocchi and Davolio 2017).

184 MOLOCH forecasts are daily provided at hourly resolution up to 2 days. The hourly

185 atmospheric forcing fields used from MOLOCH are: 2 m air temperature and relative  
 186 humidity, total cloud cover, mean sea level atmospheric pressure, meridional and zonal  
 187 10 m wind components, total precipitation rate, and the downward short-wave radi-  
 188 ation flux. The atmospheric forcing fields are horizontally interpolated at each ocean  
 189 grid node by means of a bilinear technique.

### 190 2.3.2. River boundaries

191 Freshwater is discharged into the Adriatic Sea mostly from rivers along the northern  
 192 and northwestern coasts. Due to the abundant freshwater inputs, the Adriatic Sea is  
 193 considered a dilution basin, exporting a relatively fresh water to the adjacent Ionian  
 194 Sea (Ludwig et al. 2009; Verri et al. 2018). The Po River represents the major buoyancy  
 195 input with a mean discharge rate of  $1500 \text{ m}^3 \text{ s}^{-1}$ , accounting for about one third of  
 196 the total riverine freshwater input into the Adriatic Sea.

197 Even if most of the existing oceanographic forecasting systems for the Adriatic Sea  
 198 adopt climatological values for the river boundaries (Chiggiato and Oddo 2008; Tonani  
 199 et al. 2008; Federico et al. 2017), it is well known that freshwater discharges are gen-  
 200 erally characterised by high-frequency variations. Since freshwater strongly influences  
 201 the Adriatic Sea circulation, realistic forecasts should be supplied by consistent river  
 202 discharge values. The need of operational updated discharge values is made evident  
 203 in the timeseries shown in Fig. 3, where the hourly freshwater discharges of the Po  
 204 and Isonzo rivers for the year 2016 are plotted together with their monthly mean cli-  
 205 matologies derived from Raicich (1996). Moreover, climate change is influencing flood  
 206 regimes at the continental scale, with a shift toward later floods in the northeastern  
 207 Adriatic coast (Blöschl et al. 2017).

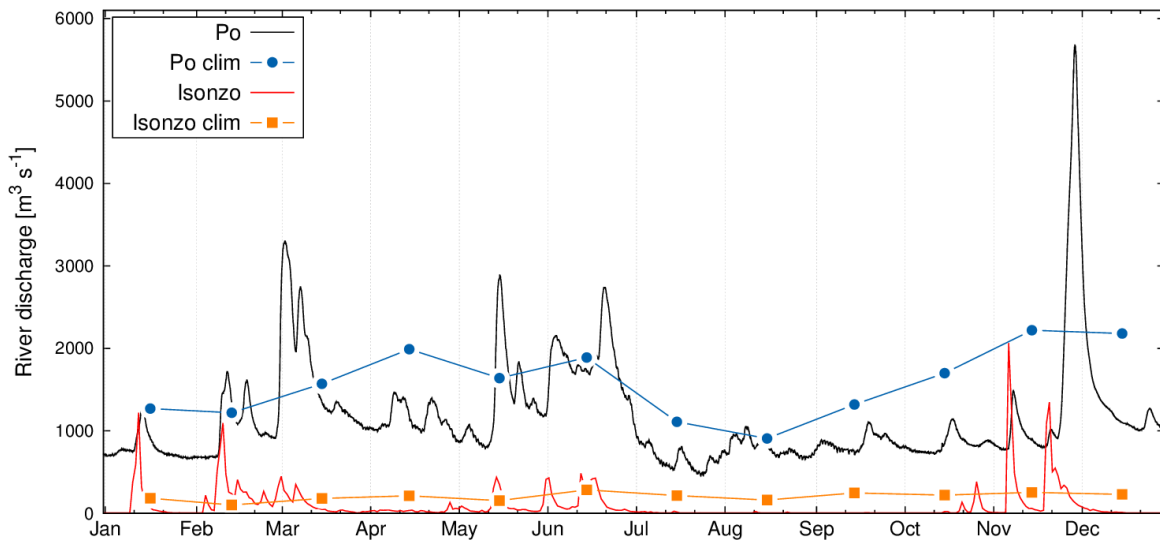


**Figure 3.** Po and Isonzo rivers discharges for the year 2016. Continuous lines indicate hourly values, while points-lines represent monthly mean climatologies.

208 In order to improve representation of the coastal freshwater discharge, in Tire-  
 209 sias the lower part of major rivers are included in the unstructured numerical mesh.  
 210 Being aware of the strong importance of land-sea interactions in coastal forecasting  
 211 (Kourafalou et al. 2015), in this study strong effort has been paid in choosing the  
 212 most accurate available river discharge conditions over the Adriatic Sea. Where avail-

213 able, daily updated river discharge values are derived from automatic hydrometric sta-  
214 tions nearest to river mouths, through calibrated stage–discharge relationships. This  
215 is the case of rivers Isonzo, Aussa, Corno, Zellina, Cormor, Turgnano, Stella, Lemene,  
216 Livenza, Piave, Brenta-Bacchiglione-Gorzone, Adige, Po, Reno, Lamone, Fiumi Uniti,  
217 Savio, Uso, Marecchia, Metauro, Esino and Tronto. The updated hydrographic levels  
218 are daily retrieved from the Civil Protection of Friuli Venezia Giulia and the Regional  
219 Environmental Protection Agencies of Veneto, Emilia-Romagna and Marche.

220 For the other rivers considered in this study (Tagliamento, Natissa, Canale dei  
221 Lovi, Sile, the tributaries of the Venice Lagoon, Po di Levante, Po di Volano, Fortore,  
222 Ofanto, Vijuse, Seman, Shkumbi, Erzen, Ishm, Mat, Bojana, Ombla, Neretva, Cetina,  
223 Krka, Zrmanja) discharges are prescribed using monthly or annual mean climatological  
224 values (Raicich 1996; Struglia et al. 2004; Ludwig et al. 2009).

225 Due to a lack of available observations, river inflow surface salinity is fixed to a  
226 constant value of 0.1 at the river boundaries. This value is lower than the ones (15-17)  
227 used by other authors (Simoncelli et al. 2011; Federico et al. 2017; Verri et al. 2018)  
228 and is justified by the fact that in Tiresias, by resolving the river-sea continuum,  
229 freshwater mixes with seawater before reaching the coast. Water temperature at the  
230 river boundaries adapts to the environmental value inside the basin.

### 231 *2.3.3. Open sea boundary*

232 Although it is clear that the model has to resolve the appropriate coastal scales, it  
233 is maybe less obvious that, for the open sea boundary conditions, the coastal model  
234 needs an upscaling effort to the basin scale. In this case the boundary conditions can  
235 be supplied by a model at a larger scale. The use of an unique numerical mesh limits  
236 the open sea boundaries to the Strait of Otranto at the southern end of the Adriatic  
237 Sea (section OA in Fig. 1). Each node of the Otranto open boundary is treated by  
238 defining water level, current velocity, salinity and water temperature.

239 The sea level and the current velocity conditions were obtained by summing the  
240 hourly tidal signal derived from the FES2012 global tidal model (Carrère et al.  
241 2012, available at [www.avisos.altimetry.fr](http://www.avisos.altimetry.fr)) and the daily water level and baro-  
242 clinic velocity predicted by the Mediterranean Forecast System (MFS, Tonani et al.  
243 2008), available via the Copernicus Marine Environmental Monitoring Service (<http://marine.copernicus.eu/>). The total water levels are imposed to the boundary  
244 nodes, while the total current velocity are nudged using a relaxation time of 3600 s.  
245 Water temperature and salinity boundary conditions are computed using the oceanog-  
246 raphic fields of MFS.

### 248 *2.4. The operational configuration*

249 The operational system chain consists of a daily cycle of numerical integrations. Every  
250 day a two-day forecast is produced, with the initial conditions from a hot start based  
251 on the Tiresias forecast of the previous day. The system performs a 2.5 day-long  
252 simulation with the first 12 hours as a spin-up time (the time interval in the past with  
253 respect to the target initial forecast day), allowing the model state to adjust to the  
254 updated river discharges and MFS fields.

255 The model is forced by the atmospheric and open sea boundary data from the  
256 MOLOCH forecasts and the MFS analysis and forecasts, respectively, for the whole  
257 simulation duration. Tiresias uses the last available river discharge data and keeps this  
258 value constant throughout the two-day forecast.



259 Since Tiresias is not assimilating observations, MFS 3D fields of sea temperature  
260 and salinity are nudged during the simulation. MFS runs on a structured grid having  
261 horizontal resolution of  $1/24^\circ$  and is operatively assimilating, through the 3DVAR  
262 scheme developed by Dobricic and Pinardi (2008), satellite sea level anomaly, satel-  
263 lite sea surface temperature and vertical temperature and salinity profiles from Argo  
264 floats. Nudging data are given for all nodes of the unstructured grid. The value of  
265 the relaxation coefficient is spatially varying over the model domain (as a function of  
266 the grid resolution) from 2 days in the open sea and increasing, thus diminishing the  
267 restoration contribution, toward the coast. Therefore, the nudging allows the model  
268 state to be reconciled with the assimilated MFS data in the open sea - limiting error  
269 growth in the forecast chain - and to fully compute the hydrodynamics along the coast  
270 and in the lagoons.

271 Tiresias runs operationally since September 2014. A two months-long simulation  
272 (July - August 2014), initialised with the MFS sea temperature and salinity fields, was  
273 performed to define the conditions for the starting state of the operational forecasting  
274 system. A similar spin-up time was used by Ferrarin et al. (2016) and McKiver et al.  
275 (2016) for simulating the Adriatic Sea hydrodynamics. The spin-up time is longer  
276 than the water renewal time in the north Adriatic lagoons (Umgiesser et al. 2014),  
277 and therefore allowed these systems to dynamically adjust after initialization from the  
278 interpolation of coarser MFS fields.

279 Tiresias runs on a Linux operating system. Its core is composed by a set of scripts,  
280 activated as soon as the MOLOCH atmospheric forcing is available, which prepare  
281 and launch each forecast simulation.

### 282 **3. Evaluation of the modelling system**

283 The application of the SHYFEM model to the Adriatic Sea has been validated in  
284 previous works reproducing correctly tidal propagation, storm surge, water flows at  
285 the lagoons' inlets and water temperature and salinity patterns along the northern  
286 coast (Bellafiore and Umgiesser 2010; Ferrarin et al. 2016; McKiver et al. 2016; Bajo  
287 et al. 2017; Ferrarin et al. 2017). However, because of the different model set-up and  
288 forcing conditions, an extensive validation of the Tiresias forecasts has been performed.

289 The validation exercises presented below aim at assessing the forecasting skills of  
290 Tiresias, but also at providing an overview of the potential applications of the numer-  
291 ical results, in both the open sea and the coastal areas.

#### 292 **3.1. Regional scale: the Adriatic Sea**

293 In addition to the wind forcing and the strong buoyancy resulting from the freshwater  
294 inputs injected by the rivers, the circulation of the Adriatic Sea is influenced by the  
295 tide (Orlić et al. 1992). Tidal dynamics are particularly evident in the northern Adri-  
296 atic Sea, where the most energetic tidal constituents - the semi-diurnal  $M_2$  and the  
297 diurnal  $K_1$  - reach amplitudes of 27 and 18 cm, respectively (Ferrarin et al. 2017). A  
298 reliable representation of the tidal dynamics is crucial, considering the role of tides in  
299 modulating buoyancy-driven river plumes, vertical mixing of the sea waters and dense  
300 water discharges (Orlić et al. 1992; Guarnieri et al. 2013; Benetazzo et al. 2014).

301 The barotropic tidal signal simulated in the Adriatic Sea using the same numerical  
302 mesh (except for some small lagoons of the Po Delta) has been recently successfully  
303 validated by Ferrarin et al. (2017). The model results were compared with the prop-

304 erties of the principal tidal waves and currents. Considering the tidal amplitudes and  
305 phases as vectors (or complex numbers), an overall measure of the match between a  
306 modelled and observed harmonic constituent is given by the vectorial difference, com-  
307 puted as distances in the complex plane (Foreman et al. 1993) The root mean square  
308 deviation of the vectorial differences, was lower than 1 cm for all constituents.

309 In order to assess the capability of the full baroclinic Tiresias system to properly  
310 reproduce the basin scale circulation in the Adriatic Sea, the forecast results were  
311 compared with the observations acquired within the MS16 cruise aboard R/V Minerva  
312 Uno in the period 7-17 December 2016. The main aim of this extensive field survey was  
313 to monitor the properties of the water column and sediment over the Italian side of  
314 the Adriatic Sea, from the Otranto Strait to the Gulf of Trieste. 67 water temperature  
315 and salinity profiles were acquired with a CTD SBE911plus probe.

316 In the validation procedure, the simulated water temperature and salinity profiles  
317 were extracted from the first day of model forecasts at the grid node nearest to the CTD  
318 station. Vertically the model results have been linearly interpolated to the observation  
319 depths. Fig. 4 maps the model performance, in terms of the difference between the  
320 average of simulated and observed values (BIAS) and the centered root mean square  
321 error (CRMSE), for the water temperature and salinity at each CTD cast.

322 The analysis of the results reveals that the operational model compares reasonably  
323 well with the measurements and reproduces the observed spatial variability of both  
324 water temperature and salinity. The average BIAS and CRMSE are 0.1 and 0.5 units,  
325 respectively, for both variables. The highest errors are found at two locations in the  
326 central Adriatic Sea (near Rimini and Pescara) and could be due to the use of the  
327 unrealistic climatological freshwater inputs. The model tends to overestimate the water  
328 temperature and salinity near Ancona. In the Gulf of Trieste the model overestimates  
329 the water temperature by 1°C and slightly underestimates the salinity. However, due to  
330 the spatial variability of errors, it is realistic to assume that the origin of discrepancies  
331 is connected with local effects.

332 To investigate the model skill over the forecast of the system, the same statistical  
333 analysis was performed using the second day of model forecasts. The error analysis  
334 showed that the model uncertainty is not increasing with the forecast validity interval  
335 (average BIAS and CRMSE of 0.1 and 0.5 units, respectively, for both variables).  
336 The good performance of the system confirms the high accuracy of the MOLOCH  
337 atmospheric forecasts and demonstrates the strength of the Tiresias approach, which  
338 combines the MFS nudging in the open sea with the high-resolution calculation along  
339 the coast. It has to be considered that in the Adriatic Sea tides strongly affect coastal  
340 dynamics (Orlić et al. 1992) and the error of reproducing the tidal signal is constant  
341 during the short term forecast (Ferrarin et al. 2013).

342 The CTD comparison was also performed in terms of 3 representative vertical pro-  
343 files, obtained averaging the CTD casts over the northern, central and southern Adri-  
344 atic Sea, respectively, according to the region subdivision illustrated in Fig. 4a. The  
345 average vertical profiles of water temperature and salinity, and their statistics in terms  
346 of CRMSE and BIAS, are illustrated in Fig. 5.

347 In the shallow northern Adriatic Sea, the observed temperature and salinity profiles,  
348 characterised by values increasing with depth, are well reproduced by the model. For  
349 both the variables the higher discrepancies with the observations were found on the  
350 surface (upper 5 m) with a CRMSE reaching 1.6 and a BIAS of 0.8 for the salinity.  
351 Such a model overestimation could be due to the impact of atmospheric and freshwater  
352 uncertainties affecting the Tiresias results in this high dynamic areas. Indeed, the  
353 CTD observations highlights that the surface layer in the northern Adriatic Sea is

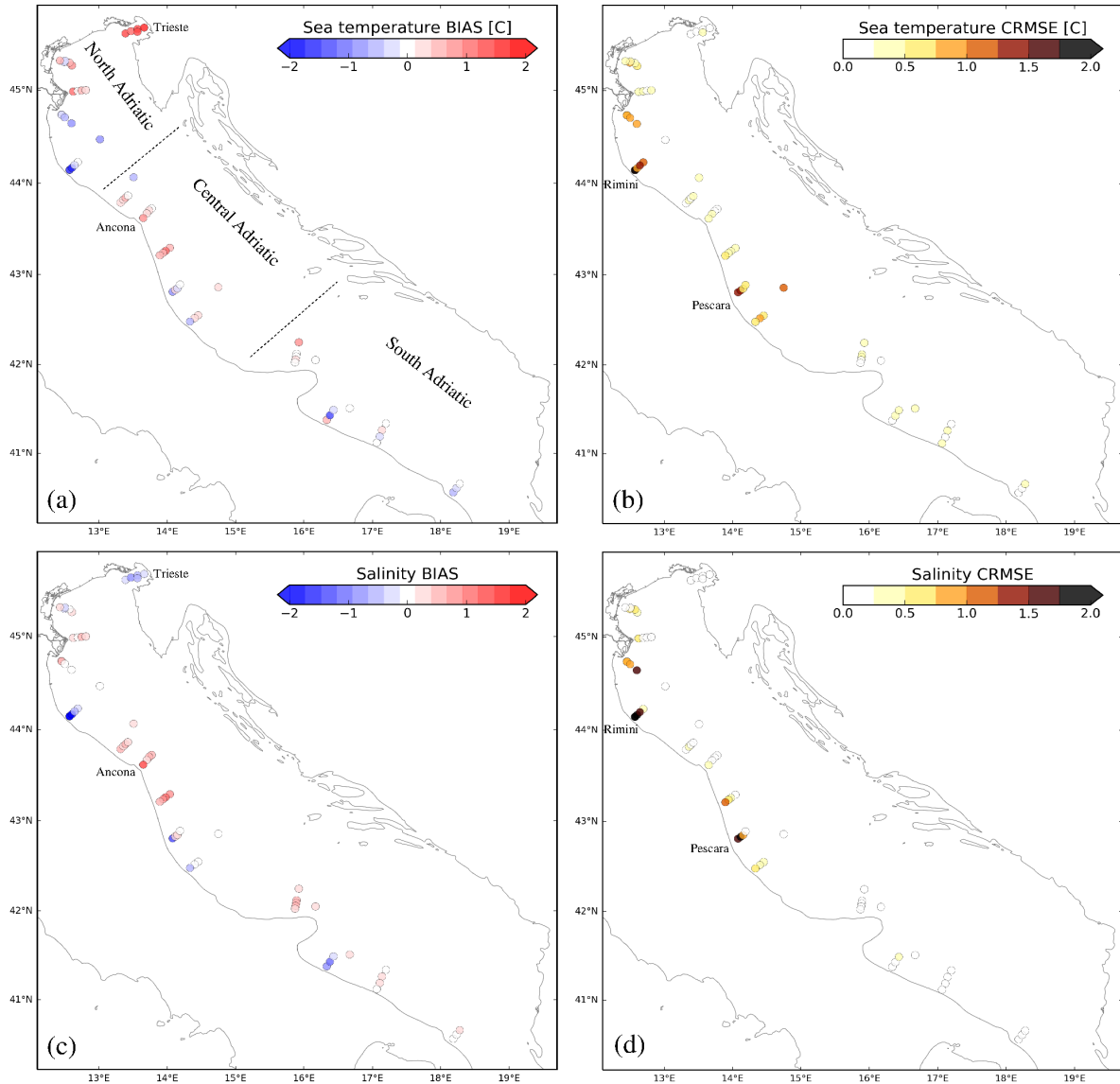


**Figure 4.** Results of the Tiresias validation with the observations of the MS16 survey in terms of vertical averaged BIAS and CRMSE for the water temperature (a, b) and salinity (c, d).

354 characterised by a standard deviation of almost 2 and 3 units for the water temperature  
 355 and salinity, respectively.

356 In the central Adriatic Sea, the model captures the average vertical structure of the  
 357 water column, characterised by colder and fresher waters in the surface. The model  
 358 overestimates by 0.5 unit both the water temperature and salinity in the upper 10 m,  
 359 and tends to enhance the mixing processes in the upper half of the water column.

360 The observed temperature profile for the southern Adriatic Sea is well reproduced  
 361 by the model. The water temperature increases till 50 m and then decreases to values  
 362 of about 15°C at the depth of 140 m. In the southern Adriatic Sea, the vertical average  
 363 Tiresias CRMSE is 0.5 °C for temperature and 0.2 for salinity. The model generally  
 364 underestimates the observed salinity by about 0.2. Such a mismatch could be due to  
 365 a too strong mixing of the upper coastal fresh waters flowing southward.

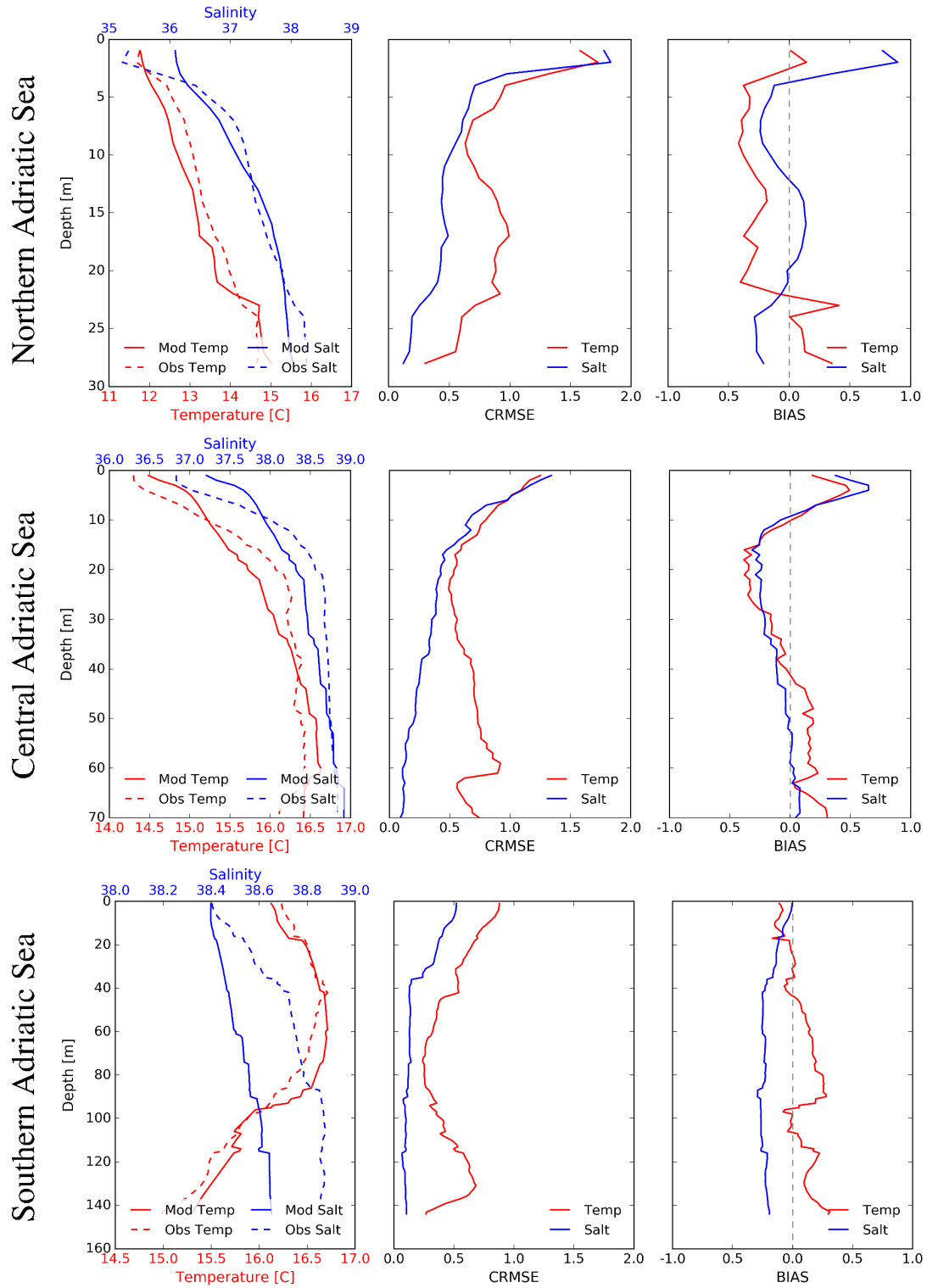


**Figure 5.** Tiresias average profiles (continuous line) of sea temperature and salinity compared with the observed ones (dashed line) in the northern, central and southern Adriatic Sea. The vertical variations of CRMSE and BIAS are also reported.

366 The high spatial variability that characterises the water masses in the Adriatic  
 367 Sea is presented in the top panels of Fig. 6, showing the distribution of the sea  
 368 surface currents, temperature and salinity fields. The maps were obtained averag-  
 369 ing the first day of the Tiresias forecasts for the period of the MS16 campaign. To  
 370 further validate the model at a regional scale, the analogous fields of the parent  
 371 model MFS (obtained by averaging the analysis and forecast results retrieved from  
 372 <http://marine.copernicus.eu/>) are presented in the bottom panels of Fig. 6.

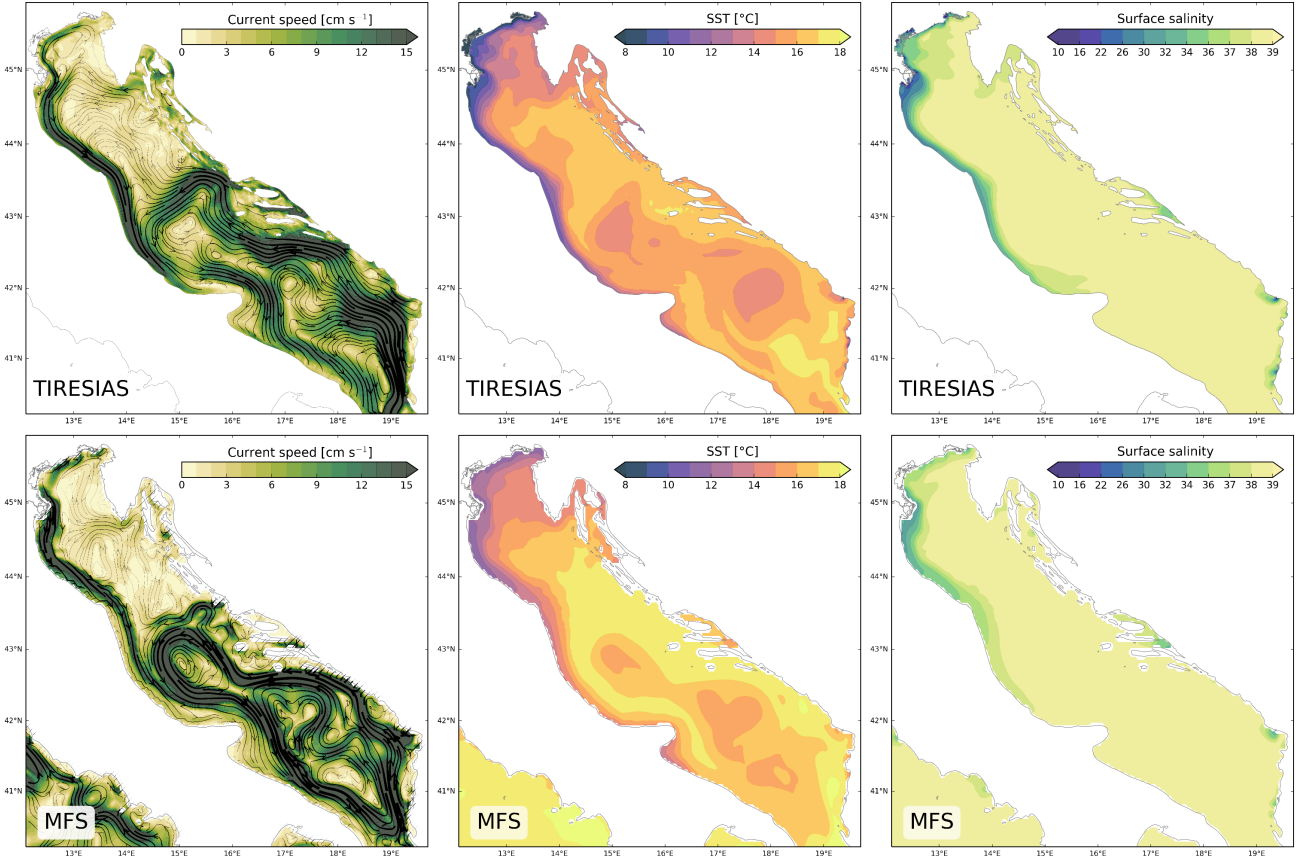


**Figure 6.** Sea surface currents, temperature and salinity computed averaging the first day of the Tiresias (top panels) and MFS (bottom panels) forecasts over the period 7-17 December 2016.

373 Tiresias correctly reproduces the main mesoscale and sub-mesoscale features in the  
 374 Adriatic Sea described by the Mediterranean Forecasting System, and consisting of  
 375 the characteristic north to south flow of cold and fresh water along the Italian coast,  
 376 the middle Adriatic and south Adriatic cyclonic gyres, the southward eastern south  
 377 Adriatic current and the northward western south Adriatic current (Bergamasco et al.  
 378 1996; Artegiani et al. 1997). In the deepest basin areas, the average circulation features  
 379 seem slightly smoother in Tiresias, compared with MFS. This aspect can be due either  
 380 to a major diffusive effect in Tiresias, to the fact that the Tiresias resolution in the  
 381 open sea is lower than MFS, or to non-linear tidal interactions, which are considered in  
 382 Tiresias and not included in MFS. The improvement in resolution in the coastal areas  
 383 permitted also to reproduce the complex circulation dynamics in the more rugged  
 384 eastern coast, composed of many islands and headlands (Orlić et al. 1992). This is  
 385 especially important during Bora events, when the strongest heat flux and wind stress

386 over the sea are concentrated in topographically controlled jets (Dorman et al. 2006;  
387 Benetazzo et al. 2014).

388 On average the sea surface temperature (SST) described by Tiresias ranges between  
389 5 and 18°C, with the lowest values found in the northern Adriatic lagoons and along the  
390 Italian coast. Tiresias SST is generally colder than the MFS one (which assimilates  
391 satellite SST data). However, the surface values extracted from the Tiresias results  
392 agree with the coastal observations acquired within the MS16 campaign (see Fig. 5).  
393 The differences with the MFS results demonstrate that over the sea surface the impact  
394 of the air-sea heat fluxes is stronger than the restoration contribution of the MFS  
395 nudging.

396 The two forecasting systems produce a similar distribution of the sea surface salin-  
397 ity, with Tiresias simulating a fresher southward surface flow along the eastern Italian  
398 coastlines and more detailed river plumes. Therefore, the high-resolution of the un-  
399 structured model in the coastal areas allows also to reproduce in details small scale  
400 circulation dynamics driven by baroclinic forcing.

## 401 **3.2. Local scales**

### 402 *3.2.1. Saltwater intrusion in the Delta of the Po River*

403 Coastal zones are dynamic and subject to changing environmental conditions caused by  
404 natural variations in climatic and oceanographic processes such as flooding, drought,  
405 storm surges and changes in sea level. In deltas and estuaries, freshwater flowing  
406 from inland areas meets with saline water from the sea. During drought conditions,  
407 saltwater penetrates far upstream increasing the salt content in aquifer and surface  
408 water (Werner et al. 2013). Moreover, since sea level is rising as a consequence of  
409 climate change, saltwater intrusion is a growing risk (Aslam et al. 2018).

410 The phenomenon of saltwater intrusion (SWI) is particularly pertinent to the Delta  
411 of the Po River, where it strongly affects farming and daily activities of the local  
412 people. By considering part of the Po River domain in the computation (up to 40 km  
413 upstream the mouth), Tiresias allows the detailed calculation of the river discharge  
414 distribution among all branches (Maicu et al. 2018). To assess the capacity of Tiresias  
415 in predicting saltwater intrusion in the main Po distributary (Po di Pila), the forecasts  
416 were compared with the salinity observed during the drought of the 2017 summer.  
417 The SAL17 field campaign was conducted on the 26<sup>th</sup> July 2017, during spring tides  
418 (the tidal range in the open sea facing the delta was about 110 cm) and low river  
419 discharge ( $490 \text{ m}^3 \text{ s}^{-1}$ ). 16 water column salinity profiles were acquired with a Idronaut  
420 Ocean Seven 316Plus multiparameter CTD sonde, starting from the river mouth and  
421 navigating 15 km upstream along the river talweg following the rising tide. The CTD  
422 probe was set for acquiring data along the water column every 10 cm. The observed  
423 salinity distribution along the transect is plotted in Fig. 7 together with the forecast  
424 results.

425 A classic estuarine dynamics (Valle-Levinson 2010), can be recognised in the Po  
426 River, with the freshwater floating on top of the denser seawater, which moves up-  
427 stream along the bottom up the river forming a wedge layer. Taking the value of 2 as  
428 the threshold for distinguishing fresh and salt waters (the salinity limit for irrigation),  
429 the observations show that the salt wedge under the fresh water penetrated into the  
430 delta up to 14 km from the river mouth. The maximum SWI extension is well fore-  
431 casted by the numerical model, which correctly reproduced the horizontal and vertical  
432 salinity gradients of the estuarine circulation. This good performance of the model was

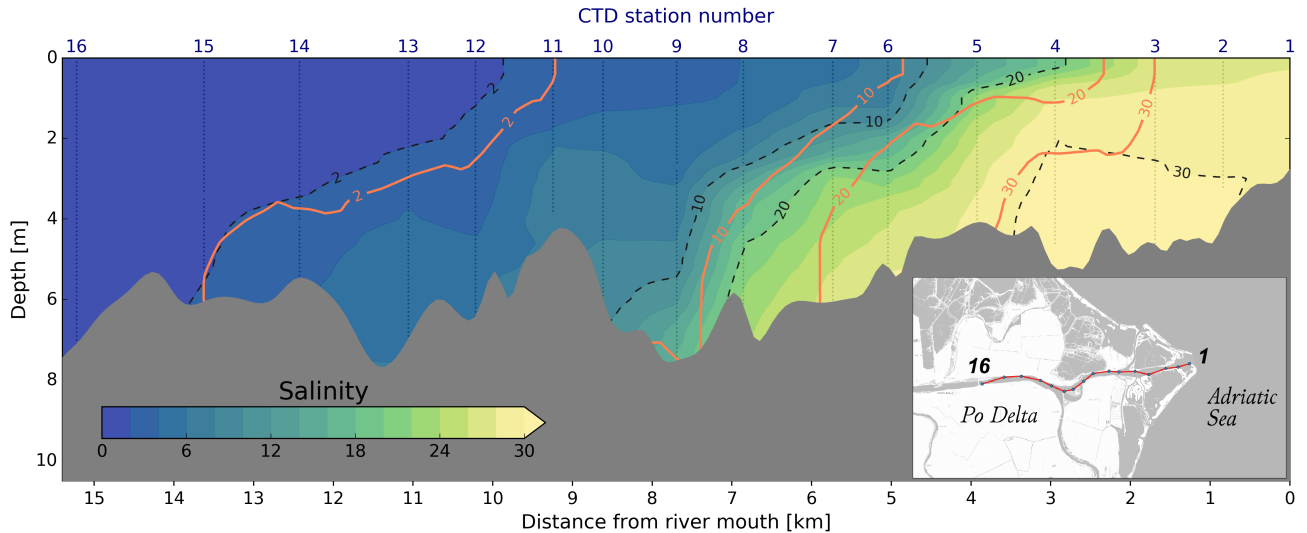


**Figure 7.** Along-river salinity section in the Po di Pila branch at flood tide (2017/07/26 12:00). Colours and black dashed contours represent the observations, while the orange continuous lines indicate the simulated values. The panel in the bottom right corner displays the survey track along the Po di Pila branch.

433 somewhat unexpected given the small scale of the SWI processes and the fact that no  
 434 data assimilation was performed in Tiresias.

435 The developed forecasting system can therefore be used for improving the manage-  
 436 ment of freshwater reservoirs and/or saltwater barriers to limit SWI in the Po Delta  
 437 (White and Kaplan 2017). The results of the Tiresias system could be useful also in  
 438 other coastal zones of the Adriatic Sea affected by saltwater intrusion, like the Adige  
 439 and Brenta rivers and large areas along the Venice coast and south of the Po Delta  
 440 (Antonellini et al. 2008; Da Lio et al. 2015).

### 441 3.2.2. Storm surge in the Venice Lagoon

442 Coastal flooding induced by storms can cause many fatalities and damages when as-  
 443 sociated to tropical cyclones and hurricanes and even in extra-tropical areas, they can  
 444 sometimes represent a serious threat (Chaumillon et al. 2017). The northern Adriatic  
 445 Sea is frequently affected by storm surge events, mainly triggered by strong south-  
 446 easterly moist and warm wind, called *Sirocco*. Although several coastal towns can be  
 447 impacted and even flooded, the main concern is for Venice, due to its artistic heritage  
 448 and historical importance. Therefore, water level prediction is of utmost importance  
 449 in Venice, since storm events often cause the flooding of the city, especially when as-  
 450 sociated with spring tides (Bajo et al. 2017). It is worth noting that with a sea level  
 451 of 110 cm (referred to local datum of Punta Salute) about 12% of the city is flooded.

452 The Tiresias forecasts were compared to the water levels observed in the open sea  
 453 at approximately 15 km offshore the lagoon inlets (the Acqua Alta oceanographic  
 454 platform, PTF in Fig. 1), and inside the Venice Lagoon (Punta della Salute, PDS in  
 455 Fig. 1). The model validation focused on the storm surge events of January 11<sup>th</sup> 2016  
 456 and June 16<sup>th</sup> 2016, when the water level in Venice reached 114 cm (Fig. 8).

457 Tiresias provided accurate water level forecasts for the analysed events, reproducing  
 458 correctly both the tidal signal (the amplitude differences are less than 0.5 cm for all  
 459 principal constituents) and the meteorological induced surge in the open sea. Addi-

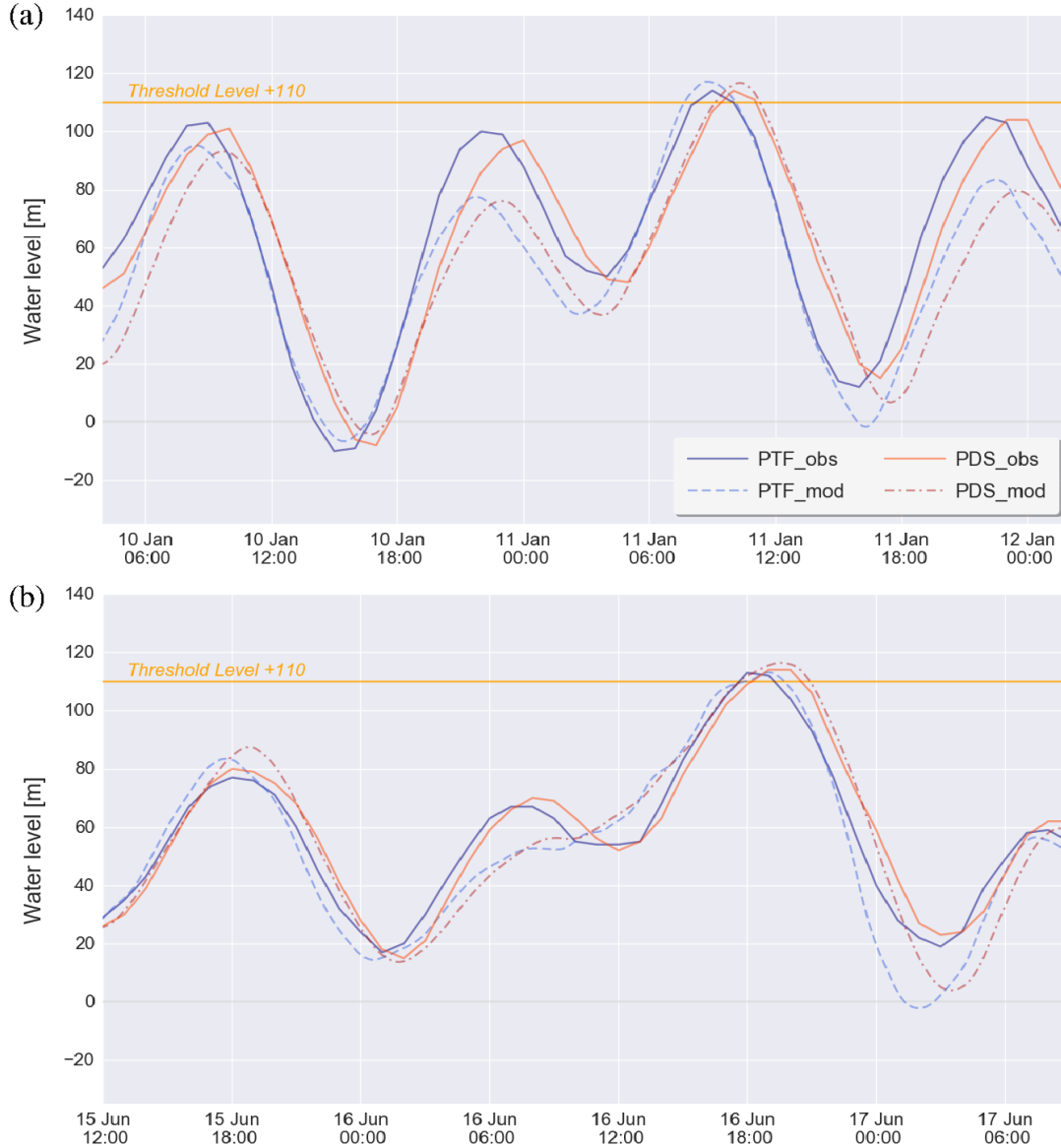


**Figure 8.** Observed (continuous lines) and forecasted (dashed lines) total water level in the Venice Lagoon (station PDS) and in the shelf facing the lagoon (station PTF), during the storm surge events of 11 January (a) and 16 June 2016 (b).

460 tionally, the numerical model accurately simulated the propagation of the total water  
 461 level inside the lagoon, where it experiences, at PDS, a delay of about 1.5 hours with  
 462 respect to PTF. For both events, the peak water level values were matched at PTF  
 463 and PDS. Due to the different meteorological conditions, the water level is amplified  
 464 within the lagoon during the storm of 16<sup>th</sup> June, while it is slightly damped during  
 465 the event of 11<sup>th</sup> January. The mismatch before and after the event can also be due to  
 466 the model error in reproducing seiches (free oscillations of the basin). In fact, most of  
 467 the great storm surge events are coupled/ followed with seiche oscillations, that start  
 468 when the forcing vanishes and may last for several days (Vilibić 2000). The correct  
 469 reproduction of these oscillations is strictly linked to the open-boundary conditions at  
 470 the Otranto Strait (Vilibić et al. 2017).



471 Accurate storm surge forecasts are crucial not only for the city of Venice (Medugo-  
472 rac et al. 2015). In particular, extreme sea levels cause flooding of large lowland coastal  
473 areas (Perini et al. 2016), and generate saline plumes that infiltrates in shallow coastal  
474 aquifer (Giambastiani et al. 2017). Due to the high-resolution of both the meteorolog-  
475 ical forcing and the oceanographic model, the Tiresias system could also be useful for  
476 predicting the probability of atmospherically induced tsunami-like waves, which occa-  
477 sionally hit the eastern Adriatic coast causing considerable damage in some harbours  
478 (Orlić 2015; Vilibić et al. 2016).

### 479 3.2.3. Particle tracking experiments

480 Lagrangian analysis provides a powerful tool to evaluate the output of ocean circula-  
481 tion models (van Sebille et al. 2018). The presented forecasting system is equipped  
482 with an off-line particle-tracking module, which simulates the trajectory of particles  
483 as a function of the hydrodynamics. The 2D particle-tracking model coupled with  
484 the hydrodynamic code has been described in Quattrocchi et al. (2016). In Tiresias,  
485 we implemented a 3D lagrangian model, where the vertical components of the turb-  
486 ulent diffusion velocity was computed using the Milstein scheme (Gräwe and Wolff  
487 2010). The horizontal diffusion was computed using a random walk technique based  
488 on Fisher et al. (1979), with the turbulent diffusion coefficients obtained by means  
489 of the Smagorinsky (1993) formulation. The off-line particle-tracking model uses the  
490 Eulerian hydrodynamic fields generated by the forecast system. The main advantage  
491 of the off-line approach is that the trajectory calculation typically takes much less  
492 computational effort than the driving hydrodynamic model.

493 The particle-tracking module of SHYFEM was successfully applied and validated by  
494 Cucco et al. (2012), Cucco et al. (2016) and Quattrocchi et al. (2016) in the Sardinian  
495 coastal waters. To validate the model in the Adriatic Sea, the lagrangian results were  
496 compared with the trajectory of a GPS-equipped drifter (<http://www.southteksl.com/index.php/products/offshore-nomad>) released the 14<sup>th</sup> May 2018 in the cen-  
497 tral Adriatic Sea (north of the city of Ancona). The drifter, floating on the surface,  
498 was equipped with a 50 cm long plastic drogue placed at 20 m depth. Therefore, the  
499 drifter provided the integral information of the currents in the upper 20 m of the  
500 water column. Drifter position was recorded at 10 min intervals and communications  
501 occurred each 4 hours.

502 In the numerical simulation, 400 particles were released (uniformly distributed on  
503 the first 20 m of the water column) at the initial drifter location. The particle-tracking  
504 module was forced by the hydrodynamic fields obtained by concatenating the first day  
505 of the Tiresias forecasts. The observed trajectories along with the paths obtained from  
506 the simulation after 13 days from the drifter release are reported in Fig. 9.

507 The particle-tracking model correctly reproduced the drifter which moved south-  
508 ward along the coast for about 110 km, with a mean speed of 10 cm s<sup>-1</sup>. The lagrangian  
509 particles moving at a depth of 4-7 m best represent the drifter behaviour. The trajec-  
510 tory absolute error of this subgroup of particles (the distances between the average  
511 position of the group of numerical particles and the corresponding drifter location;  
512 Cucco et al. 2016) remained always lower than 6 km. A remarkable result is that the  
513 uncertainty of model-predicted trajectories does not growth with the simulation time,  
514 thus confirming the robustness of the followed approach and the consistency of the  
515 previous evaluations.

516 To provide an example of the potential use of the forecast results, the particle-  
517 tracking model was applied to investigate the dispersion of the waters flowing into the  
518

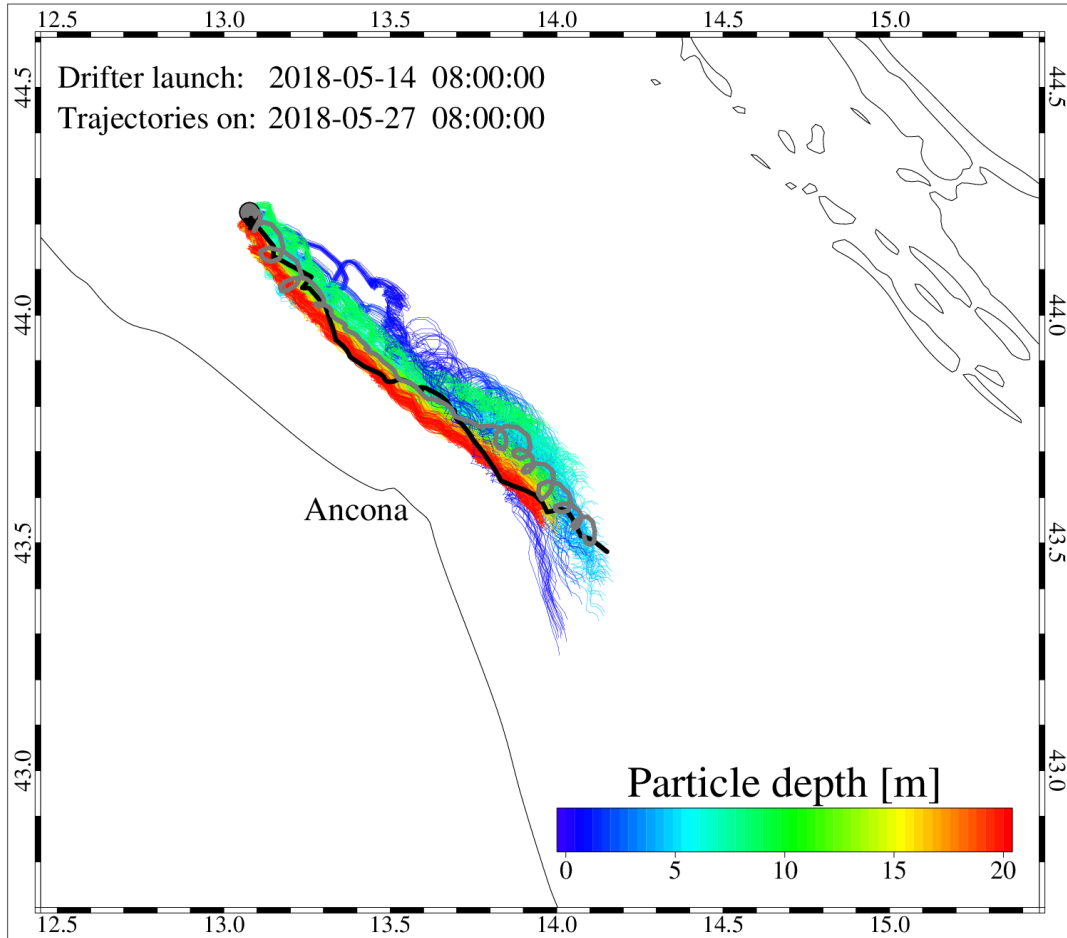


**Figure 9.** Observed (black thick line) and simulated (multicolour thin lines with the color indicating the depth of the particle) trajectories for the drifters released the 14<sup>th</sup> May 2018. The gray thick line represents the mean trajectory of the particles in the 4 to 7 m depth range.

519 Adriatic Sea from the Isonzo River (label 1 in Fig. 1). This specific site was selected  
 520 because it is well known that the Isonzo River represents the major point source of  
 521 mercury in the Gulf of Trieste and the Marano-Grado Lagoon (Covelli et al. 2007).  
 522 Therefore, even if a proper model validation cannot be carried out, since there are  
 523 no lagrangian observations available in this area, the observed spatial distribution of  
 524 suspended particulate mercury can be used to trace the Isonzo water dispersion.

525 In the numerical experiment, the fate of the Isonzo waters was simulated for river  
 526 flood of 12<sup>th</sup> January 2016, characterised by a peak discharge of  $1220 \text{ m}^3 \text{ s}^{-1}$ . Particles  
 527 were continuously released at the Isonzo River boundary during the day of the flood,  
 528 with a concentration of 1 particle per  $1000 \text{ m}^3$  of water discharged by the river. In  
 529 total 80,000 particles were released during the simulation. The lagrangian particles  
 530 had a settling velocity of  $0.5 \text{ mm s}^{-1}$  to represent the behaviour of the suspended  
 531 particulate matter.

532 The lagrangian model results (integrated over the water column) presented in Fig. 10  
 533 agree with the previous findings of Covelli et al. (2007) and Ferrarin et al. (2016), that  
 534 the river plume is generally diverted to the South-West, under the influence of the  
 535 coastal circulation, and that the tidal flux acts as a “transport belt” carrying the Isonzo

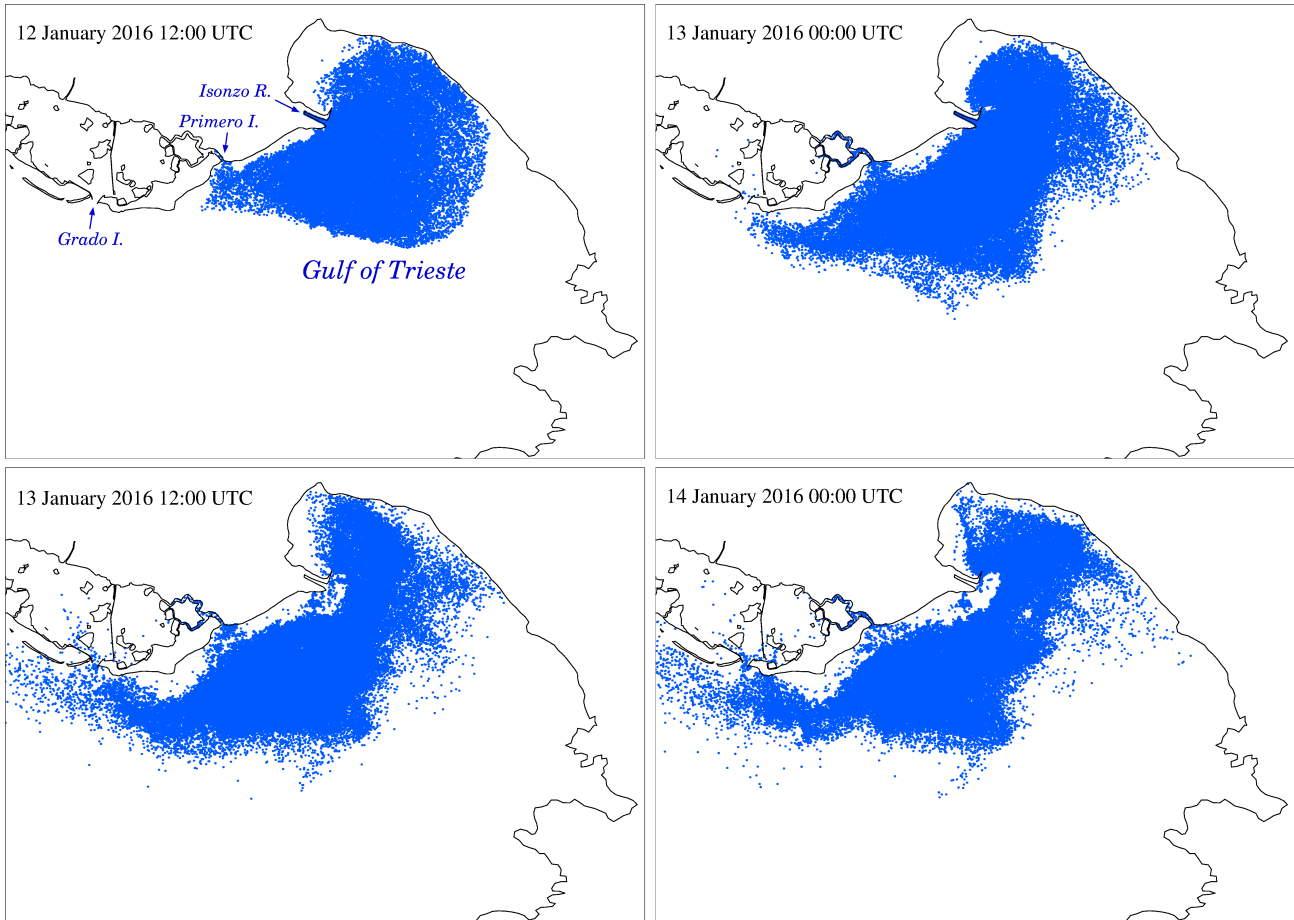


**Figure 10.** Simulated particles distribution in the Gulf of Trieste and the Marano-Grado Lagoon at intervals of 12 hours. The particles were continuously released at the Isonzo River boundary during the 12<sup>th</sup> of January 2016.

536 waters into the Marano-Grado Lagoon. In this dynamics, the Primerio and the Grado  
 537 inlets act as a preferential pathway for dissolved and suspended substances coming  
 538 from the Isonzo River to enter the eastern sector of the lagoon, where they can be  
 539 trapped. However, part of those particles can be transported out of the lagoon system  
 540 through the Grado inlet, confirming the complex exchange dynamics that characterise  
 541 this area (Turitto et al. 2018).

542 The same lagrangian methodology could also be used to help the planning and  
 543 management of the marine space (MSP) by addressing dispersion of particles and  
 544 pollutants, including those coming from accidental disposal, or for search and rescue  
 545 operations. To facilitate the use of such tools, we are developing, within the framework  
 546 of the Portodimare INTERREG Adriatic-Ionian project, a web-based particle tracking  
 547 interface for the Adriatic Sea, where the user can easily select the deployment location  
 548 and time of release of the lagrangian particles.

#### 549 4. Concluding remarks and perspectives

550 The innovative aspect of the oceanographic operational system for the Adriatic Sea  
551 presented in this study is that it accurately addresses land-sea, air-sea, and coastal-  
552 offshore interactions. These processes are taken into account in the forecasting system  
553 by adopting adjourned discharge for most of the rivers, by forcing the hydrodynamic  
554 model with high-resolution meteorological fields, and by resolving the lagoon-sea and  
555 the river-sea continuum.

556 The variable model resolution is of fundamental importance for reproducing the  
557 complex morphology of the northern Adriatic Sea. Improving modeling skills for sim-  
558 ulating coastal dynamics is a balance between trying to capture the full range of  
559 physical processes involved while at the same time introducing suitable numerical  
560 approaches for efficient simulation of the processes. The investigation on the different  
561 scales showed that Tiresias is able to correctly retain mesoscale and sub-mesoscale fea-  
562 tures as well as the coastal circulation. The improvement in resolution in the coastal  
563 areas does not only improve local dynamics by representing variability in the morphol-  
564 ogy, but also allows to reproduce in details circulation patterns driven by small-scale  
565 thermohaline and atmospheric forcing.

566 The model applications presented in this study highlight the need to take into  
567 account river mouths and coastal water bodies to properly reproduce the coastal dy-  
568 namics and the exchange processes between the different water basins. The inclusion  
569 of these coastal environments in the forecasting system is important to mankind for  
570 their ecological relevance and because many industrial, commercial, and recreational  
571 activities are concentrated in these regions.

572 Forecast products could be also useful for addressing critical and relevant coastal  
573 issues, such as marine spatial planning, maritime safety, marine pollution protection,  
574 integrated coastal zone management. Moreover, the results of the Tiresias operational  
575 system could serve to characterise the oceanographic conditions in the northern Adri-  
576 atic Sea, which has been selected as one of the study areas (Supersites) planned in  
577 the pan-European Research Infrastructure DANUBIUS-RI, the International Centre  
578 for Advanced Studies on River-Sea Systems (<http://www.danubius-ri.eu/>).

579 In the Adriatic Sea there is the need to develop an integrated observing system,  
580 similar to the ones already implemented in other part of the world, like the US In-  
581 tegrated Ocean Observing System (IOOS, Wilkin et al. 2017). With the perspective  
582 of an European Ocean Observing System (EOOS, Sparnocchia et al. 2016), the op-  
583 erational model presented in this study could be integrated with existing observing  
584 facilities (remote sensing and in-situ) and other modelling initiatives, for addressing  
585 oceanographic forecasts in both the open sea and the coastal zone. Such an observ-  
586 ing system would be invaluable for reducing errors in the initial conditions leading to  
587 better forecasts. Additionally, an international effort is also required to coordinate the  
588 production of consistent boundary conditions (i.e. rivers) for a basin-scale modelling  
589 strategy in the Adriatic Sea. To improve the oceanographic forecast, we will next ad-  
590 dress an integrated monitoring-modelling approach, with the assimilation of sea level,  
591 water temperature and salinity observations.

#### 592 Acknowledgements

593 This research was partially funded by the RITMARE (the Italian Research for the Sea)  
594 project (funded by the Italian Ministry of Education, University and Research) and the

595 Marine Strategy 2016 project (funded by the Italian Ministry for the Environment,  
596 Land and Sea; MATTM). The authors wish to thank the Civil Protection of Friuli  
597 Venezia Giulia and the Regional Environmental Protection Agencies of Veneto, Emilia-  
598 Romagna and Marche for data availability; the Veneto Region and the Consorzio di  
599 Bonifica Deltapo for supporting the SAL17 field campaign; the crew and researchers  
600 of R/V Minerva Uno for the MS16 data; Alberto Ribotti and Roberto Sorgente for  
601 providing the drifter data collected within the framework of the agreement between  
602 the Italian Ministry for the Environment, Land and Sea and the National Research  
603 Council of Italy “Realizzazione di un sistema integrato di previsione della dispersione  
604 di idrocarburi in mare e monitoraggio ambientale in corrispondenza delle piattaforme  
605 situate nell’Adriatico e nel canale di Sicilia (PNM.REG.UFF.U.0000939.17-01-2017)”.  
606 This work was inspired by the activities of the scientific community that is building  
607 the pan-European Research Infrastructure DANUBIUS-RI - The International Centre  
608 for Advanced Studies on River-Sea Systems (<http://www.danubius-ri.eu/>)

## 609 Disclosure statement

610 No potential conflict of interest was reported by the authors.

## 611 References

- 612 Antonellini M, Mollema P, Giambastiani B, Bishop K, Caruso L, Minchio A, Pellegrini L,  
613 Sabia M, Ulazzi E, Gabbianelli G. 2008. Salt water intrusion in the coastal aquifer of the  
614 southern Po Plain, Italy. *Hydrogeol J.* 16(8):1541–1556.
- 615 Artegiani A, Paschini E, Russo A, Bregant D, Raicich F, Pinardi N. 1997. The Adriatic Sea  
616 General Circulation. Part II: Baroclinic Circulation Structure. *J Phys Oceanogr.* 27(8):1515–  
617 1532.
- 618 Aslam RA, Shrestha S, Pandey VP. 2018. Groundwater vulnerability to climate change: A  
619 review of the assessment methodology. *Sci Total Environ.* 612(Supplement C):853 – 875.
- 620 Bajo M, De Biasio F, Umgiesser G, Vignudelli S, S. 2017. Impact of using scatterometer and  
621 altimeter data on storm surge forecasting. *Ocean Model.* 113:85 – 94.
- 622 Bajo M, Umgiesser G. 2010. Storm surge forecast through a combination of dynamic and  
623 neural network models. *Ocean Model.* 33(1-2):1–9.
- 624 Bellafiore D, Mc Kiver W, Ferrarin C, Umgiesser G. 2018. The importance of modeling nonhy-  
625 drostatic processes for dense water reproduction in the southern Adriatic Sea. *Ocean Model.*  
626 125:22–28.
- 627 Bellafiore D, Umgiesser G. 2010. Hydrodynamic coastal processes in the North Adriatic inves-  
628 tigated with a 3D finite element model. *Ocean Dyn.* 60:255–273.
- 629 Benetazzo A, Bergamasco A, Bonaldo D, Falcieri FM, Sclavo M, Langone L, Carniel S. 2014.  
630 Response of the Adriatic Sea to an intense cold air outbreak: dense water dynamics and  
631 wave-induced transport. *Prog Oceanogr.* 128:115 – 138.
- 632 Bergamasco A, Gačić M, Boscolo R, Umgiesser G. 1996. Winter oceanographic conditions and  
633 water mass balance in the Northern Adriatic (February 1993). *J Mar Sys.* 7(1):67 – 94.
- 634 Blöschl G, Hall J, Parajka J, Perdigão RAP, Merz B, Arheimer B, Aronica GT, Bilibashi A,  
635 Bonacci O, Borga M, et al. 2017. Changing climate shifts timing of European floods. *Science.*  
636 357(6351):588–590.
- 637 Brando VE, Braga F, Zaggia L, Giardino C, Bresciani M, Bellafiore D, Ferrarin C, Maicu F,  
638 Benetazzo A, Bonaldo D, et al. 2015. High resolution satellite turbidity and sea surface  
639 temperature observations of river plume interactions during a significant flood event. *Ocean*  
640 *Sci.* 11(6):909–920.

- 641 Buzzi A, Davolio S, Malguzzi P, Drofa O, Mastrangelo D. 2014. Heavy rainfall episodes over  
642 Liguria in autumn 2011: numerical forecasting experiments. *Nat Hazards Earth Syst Sci.*  
643 14(5):1325–1340.
- 644 Carrère L, Lyard F, Cancet M, Guillot A, Roblou L. 2012. FES2012: a new global tidal model  
645 taking advantage of nearly 20 years of altimetry. In: Ouwehand L, editor. *Proceedings of 20*  
646 *Years of Progress in Radar Altimetry Symposium.* ESA SP-710.
- 647 Chaumillon E, Bertin X, Fortunato A, Bajo M, Schneider JL, Dezileau L, Walsh JP, Miche-  
648 lot A, Chauveau E, Créach A, et al. 2017. Storm-induced marine flooding: lessons from a  
649 multidisciplinary approach. *Earth-Sci Rev.* 165(Supplement C):151 – 184.
- 650 Chiggiato J, Oddo P. 2008. Operational ocean models in the Adriatic Sea: a skill assessment.  
651 *Ocean Science.* 4(1):61–71.
- 652 Coppini G, Marra P, Lecci R, Pinardi N, Cretì S, Scalas M, Tedesco L, D’Anca A, Fazioli L,  
653 Olita A, et al. 2017. SeaConditions: a web and mobile service for safer professional and  
654 recreational activities in the Mediterranean Sea. *Nat Hazards Earth Syst Sci.* 17(4):533–  
655 547.
- 656 Covelli S, Piani R, Acquavita A, Predonzani S, Faganeli J. 2007. Transport and dispersion  
657 of particulate Hg associated with a river plume in coastal Northern Adriatic environments.  
658 *Mar Pollut Bull.* 55(10):436 – 450.
- 659 Cucco A, Quattrocchi G, Satta A, Antognarelli F, De Biasio F, Cadau E, Umgiesser G, Zec-  
660 chetto S. 2016. Predictability of wind-induced sea surface transport in coastal areas. *J*  
661 *Geophys Res Oceans.* 121(8):5847–5871.
- 662 Cucco A, Sinerchia M, Ribotti A, Olita A, Fazioli L, Perilli A, Sorgente B, Borghini M,  
663 Schroeder K, Sorgente R. 2012. A high-resolution real-time forecasting system for predicting  
664 the fate of oil spills in the Strait of Bonifacio (western Mediterranean Sea). *Mar Pollut Bull.*  
665 64(6):1186 – 1200.
- 666 Da Lio C, Carol E, Kruse E, Teatini P, Tosi L. 2015. Saltwater contamination in the managed  
667 low-lying farmland of the Venice coast, Italy: An assessment of vulnerability. *Sci Total*  
668 *Environ.* 533:356 – 369.
- 669 Davolio S, Henin R, Stocchi P, Buzzi A. 2017. Bora wind and heavy persistent precipitation:  
670 atmospheric water balance and role of air-sea fluxes over the Adriatic Sea. *Q J R Meteorol*  
671 *Soc.* 143(703):1165–1177.
- 672 Davolio S, Stocchi P, Benetazzo A, Bohm E, Riminucci F, Ravaioli M, Li XM, Carniel S.  
673 2015. Exceptional Bora outbreak in winter 2012: Validation and analysis of high-resolution  
674 atmospheric model simulations in the northern Adriatic area. *Dynam Atmos Ocean.* 71:1 –  
675 20.
- 676 Dobricic S, Pinardi N. 2008. An oceanographic three-dimensional variational data assimilation  
677 scheme. *Ocean Model.* 22(3):89 – 105.
- 678 Dorman CE, Carniel S, Cavaleri L, Sclavo M, Chiggiato J, Doyle J, Haack T, Pullen J, Grbec B,  
679 Vilibić I, et al. 2006. February 2003 marine atmospheric conditions and the bora over the  
680 northern Adriatic. *J Geophys Res Oceans.* 111(C3).
- 681 Fairall CW, Bradley EF, Hare JE, Grachev AA, Edson JB. 2003. Bulk Parameterization of  
682 Air-Sea Fluxes: Updates and Verification for the COARE Algorithm. *J Climate.* 16(4):571–  
683 591.
- 684 Federico I, Pinardi N, Coppini G, Oddo P, Lecci R, Mossa M. 2017. Coastal ocean forecasting  
685 with an unstructured grid model in the southern Adriatic and northern Ionian seas. *Nat*  
686 *Hazards Earth Syst Sci.* 17(1):45–59.
- 687 Ferrarin C, Bellaïfiore D, Sannino G, Bajo M, Umgiesser G. 2018. Tidal dynamics in the inter-  
688 connected Mediterranean, Marmara, Black and Azov seas. *Prog Oceanogr.* 161:102–115.
- 689 Ferrarin C, Maicu F, Umgiesser G. 2017. The effect of lagoons on Adriatic Sea tidal dynamics.  
690 *Ocean Model.* 119:57–71.
- 691 Ferrarin C, Roland A, Bajo M, Umgiesser G, Cucco A, Davolio S, Buzzi A, Malguzzi P,  
692 Drofa O. 2013. Tide-surge-wave modelling and forecasting in the Mediterranean Sea with  
693 focus on the Italian coast. *Ocean Model.* 61:38–48.
- 694 Ferrarin C, Umgiesser G, Roland A, Bajo M, De Pascalis F, Ghezzi M, Scroccaro I. 2016.

695 Sediment dynamics and budget in a microtidal lagoon - a numerical investigation. *Mar*  
696 *Geol.* 381:163–174.

697 Fisher HB, List EJ, Koh RC, Imberger J, Brooks NH. 1979. Mixing in Inland and Coastal  
698 Waters. (International Geophysics Series; vol. 66). San Diego, USA: Academic Press. 302  
699 pp.

700 Foreman MGG, Henry RF, Walters RA, Ballantyne VA. 1993. A finite element model for tides  
701 and resonance along north coast of British Columbia. *J Geophys Res.* 98:2509–2531.

702 Fortunato AB, Oliveira A, Rogeiro J, Tavares da Costa R, Gomes JL, Li K, de Jesus G,  
703 Freire P, Rilo A, Mendes A, et al. 2017. Operational forecast framework applied to extreme  
704 sea levels at regional and local scales. *J Oper Oceanogr.* 10(1):1–15.

705 Giambastiani BMS, Colombani N, Greggio N, Antonellini M, Mastrocicco M. 2017. Coastal  
706 aquifer response to extreme storm events in Emilia-Romagna, Italy. *Hydrol Process.*  
707 31(8):1613–1621.

708 Godunov SK. 1959. A difference method for numerical calculation of discontinuous solutions  
709 of the equations of hydrodynamics. *Matematicheskii Sbornik.* 47:271–306. Translated US  
710 Joint Publ. Res. Serv. JPRS 7226 (1969).

711 Gräwe U, Wolff JO. 2010. Suspended particulate matter dynamics in a particle framework.  
712 *Environ Fluid Mech.* 10(1):21–39.

713 Guarnieri A, Pinardi N, Oddo P, Bortoluzzi G, Ravaioli M. 2013. Impact of tides in a baroclinic  
714 circulation model of the Adriatic Sea. *J Geophys Res.* 118(1):166–183.

715 Kourafalou V, Mey PD, Staneva J, Ayoub N, Barth A, Chao Y, Cirano M, Fiechter J,  
716 Herzfeld M, Kurapov A, et al. 2015. Coastal Ocean Forecasting: science foundation and  
717 user benefits. *J Oper Oceanogr.* 8(sup1):s147–s167.

718 Ludwig W, Dumont E, Maybeck M, Heussner S. 2009. River discharges of water and nutrients  
719 to the Mediterranean and Black Sea: Major drivers for ecosystem changes during past and  
720 future decades? *Prog Oceanogr.* 80:199 – 217.

721 Maicu F, De Pascalis F, Ferrarin C, Umgiesser G. 2018. Hydrodynamics of the Po River-Delta-  
722 Sea system. *J Geophys Res Oceans.* 123:6349–6372.

723 Malguzzi P, Grossi G, Buzzi A, Ranzi R, Buizza R. 2006. The 1966 “century” flood in Italy:  
724 A meteorological and hydrological revisitation. *J Geophys Res.* 111:D24106.

725 Martin M, Balmaseda M, Bertino L, Brasseur P, Brassington G, Cummings J, Fujii Y, Lea D,  
726 Lellouche JM, Mogensen K, et al. 2015. Status and future of data assimilation in operational  
727 oceanography. *J Oper Oceanogr.* 8(sup1):s28–s48.

728 McKiver WJ, Sannino G, Braga F, Bellafiore D. 2016. Investigation of model capability in  
729 capturing vertical hydrodynamic coastal processes: a case study in the north Adriatic Sea.  
730 *Ocean Science.* 12(1):51–69.

731 Medugorac I, Pasarić M, Orlić M. 2015. Severe flooding along the eastern Adriatic coast: the  
732 case of 1 December 2008. *Ocean Dyn.* 65(6):817–830.

733 Napolitano E, Iacono R, Sorgente R, Fazioli L, Olita A, Cucco A, Oddo P, Guarnieri A. 2016.  
734 The regional forecasting systems of the Italian seas. *J Oper Oceanogr.* 9(sup1):s66–s76.

735 Oddo P, Adani M, Pinardi N, Fratianni C, Tonani M, Pettenuzzo D. 2009. A nested  
736 Atlantic-Mediterranean Sea general circulation model for operational forecasting. *Ocean*  
737 *Sci.* 5(4):461–473.

738 Oddo P, Pinardi N, Zavatarelli M, Coluccelli A. 2006. The Adriatic basin forecasting system.  
739 *Acta Adriat.* 47:169–184.

740 Orlić M. 2015. The first attempt at cataloguing tsunami-like waves of meteorological origin in  
741 Croatian coastal waters. *Acta Adriat.* 56:83 – 96.

742 Orlić M, Gačić M, La Violett PE. 1992. The currents and circulation of the Adriatic Sea.  
743 *Oceanologica Acta.* 15(2):109–124.

744 Pasarić Z, Belušić D, Chiggiato J. 2009. Orographic effects on meteorological fields over the  
745 Adriatic from different models. *J Mar Syst.* 78:S90 – S100.

746 Perini L, Calabrese L, Salerno G, Ciavola P, Armaroli C. 2016. Evaluation of coastal vulnerabil-  
747 ity to flooding: comparison of two different methodologies adopted by the Emilia-Romagna  
748 region (Italy). *Nat Hazards Earth Syst Sci.* 16(1):181–194.

- 749 Quattrocchi G, Cucco A, Antognarelli F, Satta A, Maicu F, Ferrarin C, Umgiesser G. 2016. Op-  
750 timal design of a lagrangian observing system for hydrodynamic surveys. *J Oper Oceanogr.*  
751 9(sup1):s77–s88.
- 752 Raicich F. 1996. Note on the flow rates of the Adriatic rivers. CNR, Istituto Talassografico di  
753 Trieste, Italy. Report No: 02/94.
- 754 Simoncelli S, Pinardi N, Oddo P, Mariano AJ, Montanari G, Rinaldi A, Deserti M. 2011.  
755 Coastal Rapid Environmental Assessment in the Northern Adriatic Sea. *Dynam Atmos*  
756 *Ocean.* 52(1):250 – 283.
- 757 Smagorinsky J. 1993. Some historical remarks on the use of non-linear viscosities - 1.1 In-  
758 troduutory remarks. In: B Galperin and S A Orszag, editor. *Large Eddy Simulation of*  
759 *Complex Engineering and Geophysical Flows, Proceedings of an International Workshop in*  
760 *Large Eddy Simulation.* Cambridge, UK: Cambridge University Press; p. 1–32.
- 761 Sparnocchia S, Nair R, Petihakis G, Aydoğdu A, Dobricic S, Farcy P, Martinelli M, Petersen W,  
762 Petit de la Villeon L. 2016. An interlinked coastal observatory network for Europe. *J Oper*  
763 *Oceanogr.* 9(sup1):s193–s201.
- 764 Stanev EV, Grashorn S, Zhang YJ. 2017. Cascading ocean basins: numerical simulations of  
765 the circulation and interbasin exchange in the Azov - Black - Marmara - Mediterranean  
766 Seas system. *Ocean Dyn.* 67:1003–1025.
- 767 Stocchi P, Davolio S. 2017. Intense air-sea exchanges and heavy orographic precipitation over  
768 Italy: the role of Adriatic sea surface temperature uncertainty. *Atmos Res.* 196(Supplement  
769 C):62 – 82.
- 770 Struglia MV, Mariotti A, Filograsso A. 2004. River discharge into the Mediterranean Sea:  
771 climatology and aspects of the observed variability. *J Climate.* 17:4740 – 4751.
- 772 Tonani M, Pinardi N, Dobricic S, Pujol I, Fratianni C. 2008. A high-resolution free-surface  
773 model of the Mediterranean Sea. *Ocean Sci.* 4(1):1–14.
- 774 Toro EF. 1992. The weighted average flux method applied to the Euler equations. *Philos T*  
775 *Roy Soc A.* 341(1662):499–530.
- 776 Trotta F, Fenu E, Pinardi N, Bruciaferri D, Giacomelli L, Federico I, Coppini G. 2016. A Struc-  
777 tured and Unstructured grid Relocatable ocean platform for Forecasting (SURF). *Deep-Sea*  
778 *Res Pt II.* 133:54 – 75.
- 779 Trotta F, Pinardi N, Fenu E, Grandi A, Lyubartsev V. 2017. Multi-nest high-resolution model  
780 of submesoscale circulation features in the Gulf of Taranto. *Ocean Dyn.* 67(12):1609–1625.
- 781 Turitto A, Acquavita A, Bezzi A, Covelli S, Fontolan G, Petranich E, Piani R, Pillon S.  
782 2018. Suspended particulate mercury associated with tidal fluxes in a lagoon environment  
783 impacted by cinnabar mining activity (northern Adriatic Sea). *J Environ Sci.* 68:100 – 113.
- 784 Umgiesser G, Ferrarin C, Cucco A, De Pascalis F, Bellafore D, Ghezzi M, Bajo M. 2014.  
785 Comparative hydrodynamics of 10 Mediterranean lagoons by means of numerical modeling.  
786 *J Geophys Res Oceans.* 119(4):2212–2226.
- 787 Umgiesser G, Melaku Canu D, Cucco A, Solidoro C. 2004. A finite element model for the  
788 Venice Lagoon. Development, set up, calibration and validation. *J Mar Syst.* 51:123–145.
- 789 Valle-Levinson A. 2010. *Contemporary Issues in Estuarine Physics.* Cambridge University  
790 Press.
- 791 van Sebille E, Griffies SM, Abernathey R, Adams TP, Berloff P, Biastoch A, Blanke B, Chas-  
792 signet EP, Cheng Y, Cotter CJ, et al. 2018. Lagrangian ocean analysis: Fundamentals and  
793 practices. *Ocean Model.* 121:49 – 75.
- 794 Verri G, Pinardi N, Oddo P, Ciliberti SA, Coppini G. 2018. River runoff influences on the  
795 Central Mediterranean overturning circulation. *Clim Dynam.* 50(5-6):1675 – 1703.
- 796 Vilibić I. 2000. A climatological study of the unimodal free oscillation in the Adriatic sea. *Acta*  
797 *Adriat.* 41:89–102.
- 798 Vilibić I, Šepić J, Pasarić M, Orlić M. 2017. The Adriatic Sea: A Long-Standing Laboratory  
799 for Sea Level Studies. *Pure Appl Geophys.*
- 800 Vilibić I, Šepić J, Rabinovich AB, Monserrat S. 2016. Modern Approaches in Meteotsunami  
801 Research and Early Warning. *Front Mar Sci.* 3:57.
- 802 Werner AD, Bakker M, Post VE, Vandenbohede A, Lu C, Ataie-Ashtiani B, Simmons CT,



- 803 Barry D. 2013. Seawater intrusion processes, investigation and management: Recent ad-  
804 vances and future challenges. *Adv Water Resour.* 51(Supplement C):3 – 26.
- 805 White E, Kaplan D. 2017. Restore or retreat? Saltwater intrusion and water management in  
806 coastal wetlands. *Ecosystem Health and Sustainability.* 3(1):e01258.
- 807 Wilkin J, Rosenfeld L, Allen A, Baltes R, Baptista A, He R, Hogan P, Kurapov A, Mehra A,  
808 Quintrell J, et al. 2017. Advancing coastal ocean modelling, analysis, and prediction for the  
809 US Integrated Ocean Observing System. *J Oper Oceanogr.* 10(2):115–126.
- 810 Zampato L, Bajo M, Canestrelli P, Umgiesser G. 2016. Storm surge modelling in venice: two  
811 years of operational results. *J Oper Oceanogr.* 9(sup1):s46–s57.
- 812 Zhang YJ, Stanev E, Grashorn S. 2016. Unstructured-grid model for the North Sea and Baltic  
813 Sea: Validation against observations. *Ocean Model.* 97:91 – 108.